water

MDPI

Article

Hydrogeochemistry and Precursory Anomalies in Thermal Springs of Fujian (Southeastern China) Associated with Earthquakes in the Taiwan Strait

Bo Wang [1,2,*], Xiaocheng Zhou [3,*], Yongsheng Zhou [1,*], Yucong Yan [3], Ying Li [3], Shupei Ouyang [3], Fengli Liu [3] and Jun Zhong [2]

[1] State Key Laboratory of Earthquake Dynamics, Institute of Geology, China Earthquake Administration, Beijing 100029, China
[2] China Earthquake Networks Center, Beijing 100045, China; zjadvance@126.com
[3] United Laboratory of High-Pressure Physics and Earthquake Science, Key Laboratory of Earthquake Prediction, Institute of Earthquake Forecasting, CEA, Beijing 100036, China; yanyucong2020@163.com (Y.Y.); subduction6@hotmail.com (Y.L.); ouyangshupei888@163.com (S.O.); liufengli9723@163.com (F.L.)
* Correspondence: wangbo313@163.com (B.W.); zhouxiaocheng188@163.com (X.Z.); zhouys@ies.ac.cn (Y.Z.)

Abstract: Analyzing the hydrochemical composition in thermal springs is an advantageous method for studying the coupling mechanism of the deep and shallow fluids in active fault zones. Here we conducted sampling in 30 thermal springs near fault zones in Fujian Province, and the major elements, trace elements, silica, stable isotopes (δD and $\delta^{18}O$) and strontium isotopes were tested in the laboratory. The results show that (1) the thermal springs in the study area can be divided into six types according to the content of the major elements: HCO_3-Na, $HCO_3 \cdot SO_4$-Na, Cl·HCO_3-Na, Cl-Na, Cl-Na·Ca and $HCO_3 \cdot SO_4$-Ca; (2) hydrogen and oxygen isotopes indicate that precipitation is the main source of recharge for thermal springs in the study area, and the recharge height is between 258 m and 1859 m; (3) the content of SiO_2 in the thermal spring varies from 18.1 mg/L to 59.3 mg/L. The geothermal reservoir temperature calculated is 90~226 °C, and the circulation depth is 2.9~5.4 km, except for the W10 thermal spring, whose circulation depth is 8.4 km; and (4) the $^{87}Sr/^{86}Sr$ of the thermal springs in southwestern Fujian and eastern Fujian has obviously different characteristics, indicating the influence of different rock formations on the groundwater cycle process. Additionally, a continuous measurement of the main anions and cations was performed in five thermal springs every three days since January 2020. There were obvious abnormal changes in the hydrochemical compositions, chlorine in four of the five springs, sodium at three springs, and four ions at one spring, which all showed abnormal high-value changes by 15% to 80%, and which occurred 85~168 days prior to the *M*6.1 earthquake in Hualien, Taiwan. An inspiration could be provided for obtaining effective earthquake precursor anomalies by monitoring the change in ion concentration in thermal springs.

Keywords: thermal spring; hydrochemical composition; geothermal reservoir temperature; seismic activity; Taiwan strait

check for updates

Citation: Wang, B.; Zhou, X.; Zhou, Y.; Yan, Y.; Li, Y.; Ouyang, S.; Liu, F.; Zhong, J. Hydrogeochemistry and Precursory Anomalies in Thermal Springs of Fujian (Southeastern China) Associated with Earthquakes in the Taiwan Strait. *Water* **2021**, *13*, 3523. https://doi.org/10.3390/w13243523

Academic Editor: José Virgílio Cruz

Received: 5 November 2021
Accepted: 7 December 2021
Published: 9 December 2021

1. Introduction

An active fault is a good channel for the migration of underground fluid. Meteoric water seep into the ground, enter the crust through runoff, and is heated by a geothermal source during the deep circulation process under certain structural conditions. Groundwater is affected by factors such as the storage medium and circulation conditions in the flow system, and the dissolved materials and chemical composition are dynamically changing with the groundwater cycle [1,2]. Previous studies have found that the chemical composition of groundwater changes significantly before and after moderate earthquakes [3–16]. The possible explanations for such changes include deep crustal fluid upwelling, mixing of water in different aquifers due to the rupture or crustal strain changes before and after earthquakes [17–21]. Therefore, research on the distribution pattern and the geochemical and isotopic changes in thermal springs is one of the practical ways to reveal fault activity [6,10,22–24].

Fujian is located on the southeastern edge of the Eurasian continent and connect to the Taiwan Strait, in the middle of the Zhejiang, Fujian and Guangdong uplift belts, and is part of the active continent in eastern China. According to the geological structures and the distribution of the main faults, Fujian can be divided into three regions: northern Fujian uplift belt, southwestern Fujian depression belt and eastern Fujian volcanic activity belt [25]. Although historical seismic activity in Fujian is not strong, the groundwater observation data in Fujian show that there could be abnormal changes before and after mid-strong earthquakes in the coastal areas; for example, the water temperature, element components and radon concentration of several thermal springs near the Changle-Zhaoan fault increased significantly before the 1999 Jiji 7.6 earthquake in Taiwan [26,27].

The specific aims of this study are to analyze the elemental composition and isotopic characteristics of thermal springs distributed in the different faults of Fujian, and to explore the relationship between changes in the geochemical concentration in thermal springs and the occurrence of earthquakes. It is of great significance for future use of thermal springs or groundwater observation data to determine the occurrence of mid-strong earthquakes along the coast of Fujian and Taiwan.

2. Geological Profiles

Fujian is located in the Wuyi-Daiyunlong fold belt along the southeastern coast of China. Since the Late Jurassic, large-scale intermediate-acid volcanic eruptions and Yanshanian magmatic intrusions have occurred due to the growth of the Pacific plate and the subduction and extinction of the Eurasian continent, thus forming the famous structural-magma belt and dynamic metamorphic belt along the southeast coast of China. The geomorphological pattern is characterized by denudation and weathering since the Cenozoic. There are tertiary-Quaternary terrestrial sedimentary strata in the fault basin, and marine and terrestrial formations in the coastal area [28].

From the perspective of lithosphere plate dynamics, Fujian is located in the intraplate area where the west side of the collision zone of the Pacific Plate is subducting into the Eurasian continent. Fujian and the Taiwan strait were affected by the subduction-collision compression of the Philippine Sea plate to the northwest, which resulted in many dynamics process successively developing, such as the strong interplate seismic zone in eastern Taiwan, the marginal seismic zone in western Taiwan and the intraplate seismic zone along the southeast coast. The distribution of seismic belts in Fujian is closely related to the Quaternary active faults, which consist of three larger active faults, namely, the Shaowu-Heyuan fault, Zhenghe-Haifeng fault and Changle-Zhaoan fault; all of these faults have spread in the NNE direction. Figure 1 show the simplified geological map and historical earthquakes, where the gray circles represent $M_s \geq 5$ historical earthquakes, and the red circles represent $M_s \geq 3$ earthquakes since 1970 (Figure 1).

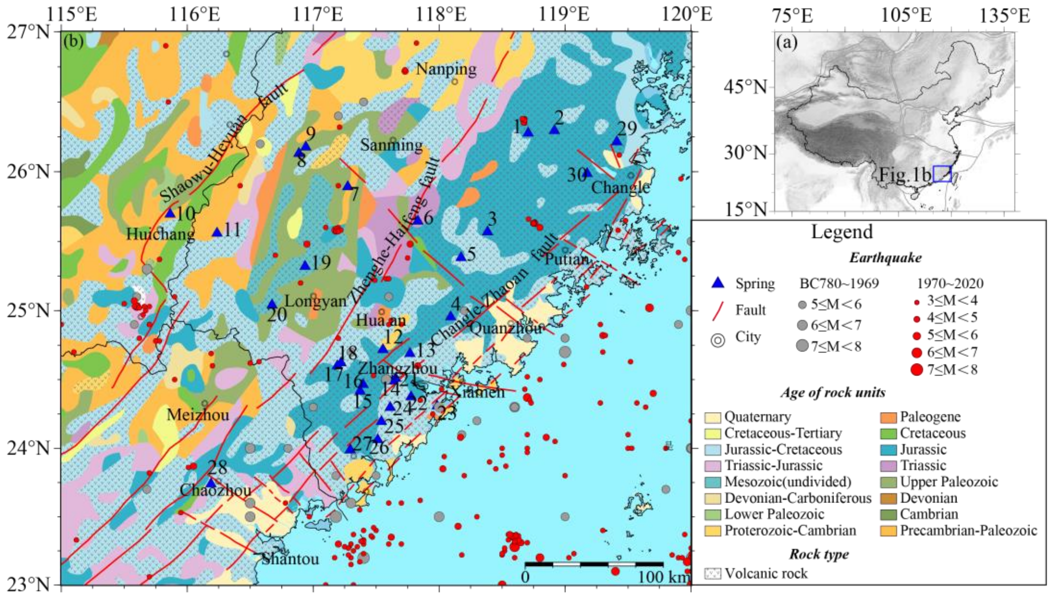

Figure 1. (**a**) Localization of the study area. (**b**) Geological map showing the location of the thermal springs, historical earthquakes and major faults of Fujian.

3. Data and Method

A total of 30 thermal springs were sampled in January 2020. Temperature, pH, conductivity, major elements, trace elements, silicon dioxide, strontium isotopes, hydrogen and oxygen isotopes of the sampled springs were analyzed (see Tables S1 and S2 for data and Figure 1 for sample locations). The determination of the major elements in thermal springs was completed by a Dionex ICS-900 ion chromatograph (Thermo Fisher Scientific Inc., Sunnyvale, CA, USA) and AS40 autosampler instruments with a detection limit of 0.01 mg/L (Dionex Corporation, Sunnyvale, CA, USA) in the Key Laboratory of Earthquake Prediction Institute of China Earthquake Administration [29]. HCO_3^- and CO_3^{2-} were measured with a ZDJ-3D potentiometric titrator through standard titration procedures, and the measurement errors of the anion and cation are both less than 5%. The analysis of the trace elements was completed at the Test Center of the Institute of Nuclear Industry Geology, using an element-type inductively coupled plasma mass spectrometer ICP-MS (PerkinElmer, Waltham, MA, USA) [30]. The gas isotope mass spectrometer MAT253 (Thermo Fisher Scientific Inc., Sunnyvale, CA, USA) was adopted to analyze the hydrogen and oxygen isotopes, where the test errors of δD and $\delta^{18}O$ were less than one thousandth and two ten thousandths, respectively [31]. The inductively coupled plasma emission spectrometer Optima-5300 DV (PerkinElmer, Waltham, MA, USA) was used to detect the concentration of silicon dioxide. The analysis of strontium isotopes was done by a Phoenix thermal ionization mass spectrometer (Thermo Fisher Scientific Inc., Sunnyvale, CA, USA) [32].

4. Results and Discussion

The water temperature of the thermal springs in the study area varies from 25 °C to 90 °C. The pH of these thermal springs is between 7.01 and 8.23, with an average of 7.75 and median of 7.82. The electrical conductivity varies from 185.4 µS/cm to 18150µS/cm. The main anions and cations in the thermal springs are HCO_3^-, SO_4^{2-}, and Na^+, with some exceptions. The ranges of hydrogen and oxygen isotopes in the thermal spring samples are $-56.3‰ \leq \delta D \leq -37.6‰$ and $-8.7‰ \leq \delta^{18}O \leq -5.5‰$, respectively. Silica contents vary from 18.1 mg/L to 59.3 mg/L. The $^{87}Sr/Sr^{86}$ value is 0.706–0.726. The concentrations of trace elements are extremely low, except for Sr and Li in a small number of the thermal springs.

The chemical composition of thermal springs along the fault is one of the important means to reveal the activity of the fault. The concentrations of F^-, Cl^-, SO_4^{2-}, Na^+,

SiO_2 and trace elements Li or Sr were very low in the shallow groundwater, but higher in geothermal water that has undergone deep circulation. Certain ion ratios (Na^+/K^+, Na^+/Ca^{2+}) in geothermal water, and even the content of a certain single component (Si) can indicate its circulation depth. Through the ratio of rubidium and strontium isotopes, the ambient petrophysical composition in the cycle of the thermal spring can be determined, and also the thermal spring circulation time can be calculated [33,34].

4.1. Geochemical Characteristics of Major Elements

It can be seen from the calculation results that Na is the main cation while HCO_3 and SO_4 are the main anions in most springs. The 30 samples could be divided into 7 types according to the chemical constituent in the springs: HCO_3-Na, $HCO_3{\cdot}SO_4$-Na, $HCO_3{\cdot}SO_4$-Na·Ca, Cl-Na·Ca, Cl-Na, $SO_4{\cdot}HCO_3$-Ca and $Cl{\cdot}SO_4{\cdot}HCO_3$-Na (Table S1 and Figure 2). The chemical constituent in the thermal springs is correlated with the surrounding rock. The anions of thermal springs on the southeast Fujian fault zone are dominated by sodium bicarbonate, indicating that most thermal springs may be in the metamorphic rock area. All the thermal springs in the southwestern Fujian depression zone contain a certain concentration of sulfate ions, indicating that these thermal springs may be in the sedimentary rock area; moreover, sulfate minerals may dissolve in the thermal springs due to the water–rock reaction during the deep circulation of groundwater. There are also some exceptions; for example, calcium is the main cation in the W30 thermal spring, and the milligram equivalent accounts for 79.4%. There is a positive exponential correlation between the calcium concentration in the thermal spring and the saturation index of calcite and dolomite, indicating that the ambient lithology is dominated by these two kinds of rocks. The anion is dominated by chloride, whose milligram equivalent is more than 90% in W21, W22, W23 and W26 thermal springs, and the calcium concentration is higher than that of other thermal springs. The thermal springs have a relatively low ionic salinity (7.2~30 meq/kg) with the exception of the four springs whose value range from 47.2 to 398.8 meq/kg, as indicated by the correlation plot of Na+K vs. Ca+Mg (Figure 3). Three of these four thermal springs are located close to the sea, and the element composition and concentration are almost the same as that of seawater. The higher concentrations of Ca^{2+} and Mg^{2+} are probably due to mixing with Ca- and Mg-rich cold waters in shallow aquifers or mixing with seawater, as they also have higher concentrations of Cl^-. It is speculated that the groundwater in these regions may be affected by seawater invasion.

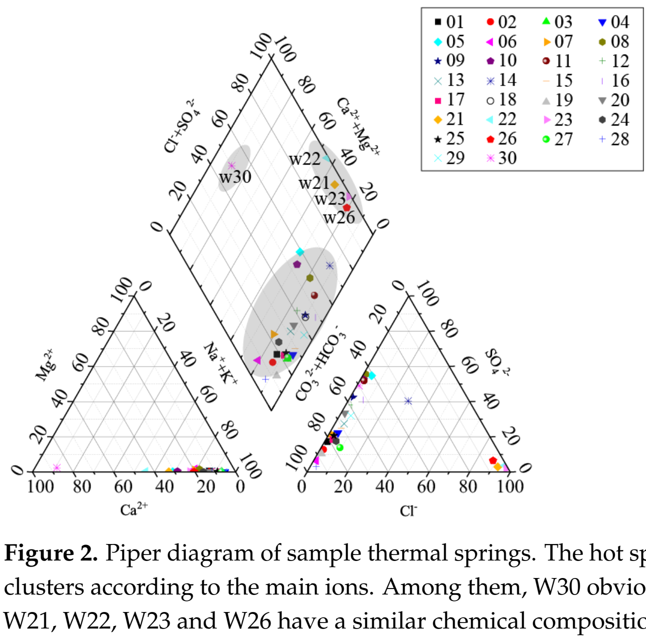

Figure 2. Piper diagram of sample thermal springs. The hot spring samples can be divided into three clusters according to the main ions. Among them, W30 obviously deviates from the others, whereas W21, W22, W23 and W26 have a similar chemical composition; the other 25 samples form a unique and the major category.

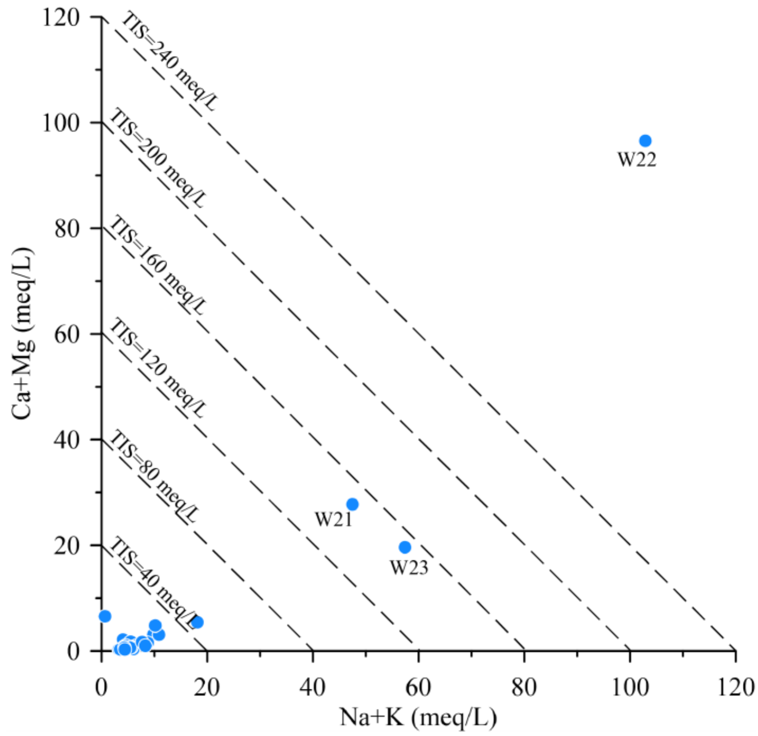

Figure 3. Correlation plot of Na+K vs. Ca+Mg for the sample thermal springs in the research area, also showing the iso-ionic-salinity (TIS) lines for reference.

4.2. Geochemical Characteristics of Trace Elements

The element content of the hot spring depends on the water–rock reaction during the deep circulation of groundwater; therefore, the trace elements in thermal springs can show the degree of water–rock reaction to a certain extent (Table S2). The enrichment factor is the degree of enrichment of a certain element in a specific geological body, and the source of the trace elements in a thermal spring can be qualitatively determined according to the enrichment factor [35]. The calculation formula of the enrichment factor is

$$EF_i = (C_i/C_R)_w/(C_i/C_R)_r$$

where C_R is the selected reference element content, C_i is the element content in the sample, w is the element concentration in the water sample and r is the element concentration in the rock.

Taking the average value of trace elements of the typical syenogranite in southwestern Fujian as the reference value [25], Ni was selected as the reference element [36], and the normalized trace element values are shown in Table 1. It can be seen that the enrichment factors of Mo and Sr in most thermal springs in the study area are greater than 1, while the enrichment factors of the other elements are extremely low. When the value of the enrichment factor is less than 1, it means the element is dispersed. The higher Mo and Sr contents have the characteristics of granite origin, especially Mo, which is a typical element of granite source and a high-temperature mineralization element. It indicates that the granite has a greater contribution to the chemical characteristics of the thermal springs. There is no modern volcanic activity in the study area, so it is inferred that the granite porphyry bodies has not yet been completely cooled.

The Sr concentration is higher compared with other trace elements in thermal springs (Table S2). In particular, the concentration of Sr in the W21, W22, W23 and W26 thermal springs is higher, and the measurement is 24 mg/L, 44 mg/L, 14 mg/L and 5 mg/L (Figure 4), while Sr in seawater is about 8 mg/L [37]. Strontium has a better mobility and higher concentration in chloride-type or sulfuric acid-type water. Thus, there may be a wide distribution of deep chloride brine in the stratum in the area where such thermal springs are located. In addition, the strontium isotope can reflect the formation lithology the thermal springs flowed through. The $^{87}Sr/^{86}Sr$ of carbonate and sulfate weathering sources was 0.708, and the $^{87}Sr/^{86}Sr$ of the aluminosilicate weathering sources varied between 0.716 and 0.72 [38,39]. The ratio of $^{87}Sr/^{86}Sr$ in the thermal springs in the study area ranged from 0.706 to 0.726, and there were significant differences in the strontium isotopes of the thermal springs in the different regions. The strontium isotope of the thermal springs in the southwestern Fujian depression area is relatively high, which is closer to the source of aluminosilicate weathering, while that in the Eastern Fujian volcanic activity belt is relatively low, indicating that it is closer to the source of carbonate and sulfate. The distinction in the strontium isotopes also manifests the differences in the formation lithology in the two regions.

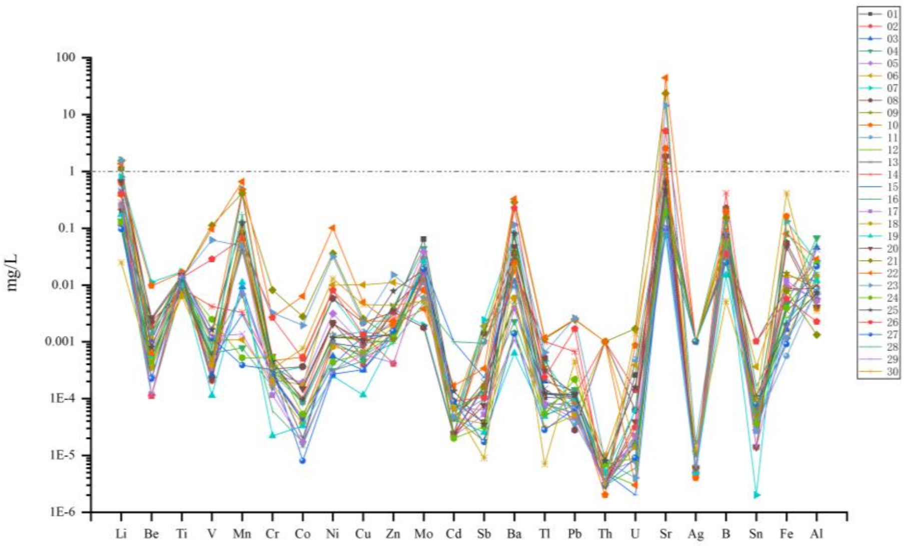

Figure 4. The content of trace elements in the sampled thermal springs.

Table 1. The enrichment factor of the trace elements.

Thermal Spring Code	Element Enrichment Factor												
	V	**Cr**	**Co**	**Cu**	**Zn**	**Mo**	**Ba**	**Pb**	**Th**	**U**	**Sr**	**Ag**	**Sn**
W01	0.04	0.08	0.09	0.17	0.12	120.12	0.12	0.00	0.00	0.07	18.98	/	/
W02	0.04	0.11	0.06	0.28	0.13	125.66	0.27	0.01	/	0.09	26.78	/	0.02
W03	0.08	0.18	0.09	0.39	0.17	130.75	0.54	0.03	0.00	0.02	19.87	0.34	0.06
W04	0.35	0.23	0.06	1.00	0.99	581.06	0.07	0.05	0.00	0.04	15.21	1.33	0.08
W05	0.02	0.04	0.07	0.19	0.05	50.26	0.04	0.00	0.00	0.00	10.63	0.06	0.00
W06	0.02	0.01	0.02	0.68	0.08	3.27	0.01	0.00	0.00	0.02	1.48	0.02	0.02
W07	0.01	0.02	0.07	0.14	0.05	1.31	0.13	0.00	0.00	0.00	13.63	0.04	0.00
W08	0.02	0.03	0.08	0.26	0.04	1.26	0.06	0.00	/	0.01	19.32	0.03	0.00
W09	0.05	0.11	0.08	0.54	0.11	17.88	0.29	0.00	0.00	0.01	25.92	0.17	0.01
W10	0.03	0.02	0.08	0.19	0.02	4.11	0.03	0.00	0.00	0.07	18.81	0.02	0.00
W11	0.07	0.09	0.08	0.80	0.07	36.32	0.08	0.00	0.00	0.24	25.45	0.15	0.01
W12	0.07	0.11	0.09	0.57	0.06	47.45	0.56	0.00	0.00	0.00	26.39	0.15	0.01
W13	0.10	0.15	0.03	0.56	0.32	60.47	0.05	0.01	0.00	0.04	19.40	0.20	0.03
W14	0.34	0.08	0.06	0.27	0.10	34.34	0.08	0.03	0.00	0.00	28.60	0.10	0.01
W15	0.21	0.30	0.12	2.21	0.24	243.24	0.34	0.03	0.00	0.00	35.79	0.49	0.05
W16	0.51	0.09	0.07	2.16	0.27	329.97	0.18	0.03	0.00	0.01	51.87	/	0.25
W17	0.06	0.05	0.02	0.40	0.09	51.29	0.04	0.01	0.00	0.01	15.92	0.19	0.02
W18	0.08	0.10	0.05	0.54	0.16	78.69	0.07	0.01	/	0.01	22.14	/	0.02
W19	0.08	0.04	0.16	0.31	0.35	438.14	0.03	0.04	0.00	0.15	18.19	0.75	0.05
W20	0.02	0.12	0.09	0.34	0.05	33.65	0.23	0.01	0.00	0.01	18.26	0.11	0.00

Table 1. *Cont.*

Thermal Spring Code	Element Enrichment Factor												
	V	**Cr**	**Co**	**Cu**	**Zn**	**Mo**	**Ba**	**Pb**	**Th**	**U**	**Sr**	**Ag**	**Sn**
W21	0.54	0.10	0.09	0.05	0.00	1.49	0.08	0.01	/	0.03	39.73	0.01	0.00
W22	0.17	0.01	0.07	0.03	0.00	0.15	0.03	0.00	/	0.00	26.52	/	0.00
W23	0.34	0.05	0.07	0.05	0.03	0.73	0.04	0.01	0.00	0.00	27.50	0.02	0.00
W24	0.97	0.52	0.14	0.93	0.22	171.95	0.03	0.05	0.00	0.01	26.64	/	0.04
W25	0.24	0.17	0.10	0.72	0.49	65.52	0.70	0.01	0.00	0.08	24.31	0.19	0.04
W26	0.62	0.15	0.07	0.11	0.00	9.18	0.28	0.02	0.00	0.00	39.09	/	/
W27	0.75	0.53	0.04	0.82	0.42	289.24	0.05	0.03	0.00	0.02	22.32	/	0.13
W28	0.13	0.18	0.10	0.37	0.07	20.08	0.20	0.01	0.00	0.01	20.86	/	0.02
W29	0.70	0.25	0.06	1.35	0.10	207.69	0.04	0.02	0.00	0.04	21.86	0.74	0.02
W30	0.01	0.01	0.07	0.24	0.02	1.65	0.02	0.00	0.00	0.07	6.21	0.03	0.00

4.3. Stable Isotope Characteristics and Origin of Thermal Springs

Isotopic characteristics of the groundwater can provide a theoretical basis for analyzing the recharge source of groundwater. The measured values of δD and $\delta^{18}O$ in the thermal springs ranged from −37.6‰ to −56.30‰ and from −5.5‰ to −8.7‰, respectively. The δD–$\delta^{18}O$ relationship diagram (Figure 5) shows that the 30 sample points are scattered near the Global Meteoric Water Line (GMWL) and the Local Meteoric Water Line in Fujian (LMWL) [40–45], indicating that precipitation is the main source of recharge for thermal springs.

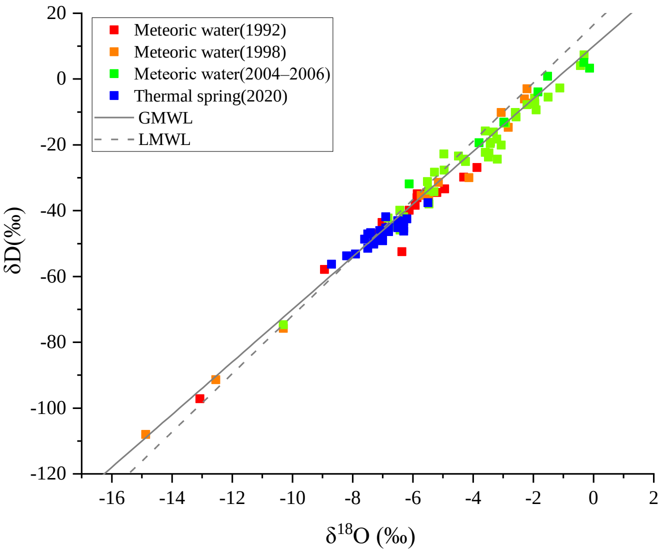

Figure 5. Scatter plot of the δD and $\delta^{18}O$ values from the sampled thermal springs and meteoric water. The red, orange and green squares represent the δD vs. $\delta^{18}O$ for the local precipitations of 1992, 1998 and 2004–2006, respectively [43–45], and the blue square represents the δD vs. $\delta^{18}O$ for the thermal springs in this work.

Based on the empirical statistical formula of groundwater recharge elevation and oxygen isotope in southeast China, $\delta^{18}O = -0.002*altitude - 4.983$ [46], the recharge elevations of the considered thermal springs in the study area were calculated, with a result ranging from 258 m to 1859 m. Faults provide tectonic precondition for the deep circulation of groundwater, so the scales and patterns of the fault play a certain role in controlling the formation of thermal springs. In addition, a larger hydraulic head difference is also a necessary condition for deep circulation of groundwater, which may be one description for the lack of thermal springs in northeast Fujian.

4.4. Geothermal Reservoir Temperature and Circulation Depth

The Na-K-Mg ternary diagram can be used to indicate the degree of water–rock reaction and the equilibrium temperature of geothermal water [47]. It can be seen that 19 sample thermal springs are found in the field of the partially equilibrated waters, whereas the other 11 thermal springs fall in the field of immature waters (Figure 6). Owing to the plethora of water geothermometers and their inevitable drawbacks [48–51], we selected a variety of geothermometers in this work to optimize their use and find the most suitable one. Most of the thermal springs in the study area are in an immature condition or in partial equilibrium condition, and all ionic geothermometers are actually functions of not only temperature but also of P_{CO2} and ionic salinity [52–54], so the cation geothermometer is not suitable for estimating the equilibrium temperature. Silica functions are affected by the mixture of cold water in shallow aquifers and other effects; consequently, we use the mixing model to compute the geothermal reservoir temperature and apply to the calculation of circulation depth. The temperature of the cold spring water in the study area, 18 °C, was used as the standard value for the local cold spring in the calculations [55]. The results computed through direct application of multi-geothermometers were shown in Table 2.

As the thermal springs are recharged by meteoric water, the geothermal reservoir temperature generally increases with the increase of the depth of thermal spring water circulation. The circulation depth of the thermal spring can be calculated by the following formula:

$$D = (t_R - t_{cold})/g + h$$

where D is the circulation depth (km) and g is the geothermal gradient (°C/km), which is set to 25 °C/km in the calculation in this paper [56]; t_R is the geothermal reservoir temperature through the silica-enthalpy mixing model (°C); t_{cold} is the temperature of the local cold spring (°C); h is the distance from the ground to underground constant temperature zone (km); and 30 m was taken in our calculation [55].

The geothermal reservoir temperature of the thermal spring in the study area varies from 90 °C to 226 °C. The circulation depths of the thermal springs were between 2.9 and 5.4 km, except for W10 thermal spring, with a circulation depth of 8.4 km (Table 2).

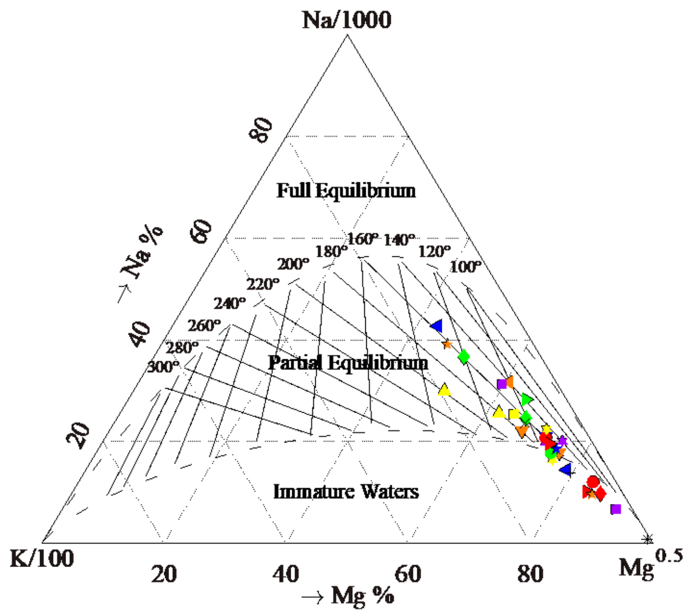

Figure 6. Na-K-Mg ternary diagram of the sampled thermal springs.

Table 2. Apparent equilibrium temperatures computed through multi-geothermometers for the samples collected from the thermal springs of Fujian.

Thermal Spring Code	Qz °C	Qz,msl °C	SiO_2 °C	SiO_2,msl °C	Na-K,F °C	Na-K,G °C	K-Mg °C	K-Mg,msl °C	Mixing Model °C	Circulation Depth km
W01	86	89	60	67	135	155	74	75	138	4.8
W02	96	98	71	77	142	162	90	90	141	5
W03	105	106	82	86	162	180	114	113	121	4.2
W04	100	101	75	80	140	159	101	100	118	4
W05	91	93	65	71	161	179	91	91	118	4
W06	91	93	65	71	150	169	65	66	127	4.4
W07	110	110	87	90	173	191	85	85	153	5.4
W08	79	83	52	60	169	187	81	82	107	3.6
W09	103	104	80	84	164	183	97	97	132	4.6
W10	96	98	71	76	155	174	95	95	226	8.4
W11	73	77	45	54	137	157	93	93	94	3.1
W12	80	83	53	61	143	163	94	94	102	3.4
W13	86	89	60	67	146	165	73	74	118	4
W14	78	82	51	59	120	140	101	101	118	4
W15	89	91	63	69	149	168	107	106	122	4.2
W16	80	84	53	61	118	139	95	95	90	2.9
W17	86	89	59	67	141	161	91	91	118	4
W18	78	81	50	59	119	139	83	83	96	3.2
W19	97	98	72	77	140	159	94	94	153	5.4
W20	101	102	77	81	159	178	106	105	140	4.9
W21	90	92	64	70	182	199	133	131	150	5.3
W22	89	92	63	70	140	159	120	119	116	4
W23	79	83	52	60	136	156	128	126	95	3.1
W24	84	87	57	64	129	149	106	105	98	3.2
W25	91	93	66	72	144	163	94	94	122	4.2
W26	82	85	55	63	143	162	126	124	136	4.8
W27	82	85	55	63	127	147	91	91	105	3.5
W28	87	90	61	68	161	180	89	90	95	3.1
W29	95	97	70	76	147	166	103	102	110	3.7
W30	60	66	31	41	172	190	27	29	140	4.9

Qz = no-steam-loss quartz geothermometer [49]; Qz,msl = maximum-steam-loss quartz geothermometer [49]; SiO_2 = no-steam-loss silica(quartz/chalcedony) geothermometer [48]; SiO_2 = maximum-steam-loss silica(quartz/chalcedony) geothermometer [48]; K-Mg = no-steam-loss K-Mg geothermometer [47]; K-Mg,msl = maximum-steam-loss K-Mg geothermometer [47]; Na-K,F = Na-K geothermometer [50]; Na-K,G = Na-K geothermometer [47]. The mixing model is from Fournier and Truesdell [51].

4.5. Geothermal Characteristics and Seismic Activity

Geothermal energy and earthquakes are different manifestations of the energy release inside the earth. An earthquake is a sudden release of crustal stress while a thermal spring is another manifestation. In addition, the physical and chemical reactions between the hot water and surrounding rocks in the groundwater cycle process could have a significant impact on seismic activity. Fujian is located at the intersection of the Eurasian plate, the Pacific plate and the Philippine plate. Collision and subduction of the continental margin of southeastern China affected the formation of thermal springs and the distribution of earthquakes; this can be seen from Figure 1, where the seismicity in Fujian is unevenly distributed. There are few earthquakes in the north of Fujian, especially in the northeast, while the distribution of earthquakes of *M*5 or higher has increased significantly in the southeastern Fujian and the Taiwan Strait. The northwest and northeast trending faults are intersected in the southeastern Fujian, with many fault branches, which is a good channel for underground hot water transportation and storage. This partly explains why thermal springs are relatively dense in this area [57].

The distribution of thermal springs is closely related to active faults, but the relationship between the underground hot water and earthquakes is more complicated. Some studies have shown that the infiltration of hot water could decrease the effective normal stress and reduce the shear strength of the rock, which causes weakening behavior of the fault [17,58]. Therefore, if the circulation of underground hot water covers the deep layer of the fault, the weakening effect of the hot water to the fault will be enhanced, the strength of the fault will be significant reduced, and the fault will more easily slip, resulting in high-frequency small and medium earthquakes. On the contrary, if the circulation depth of the underground hot water is only limited to the shallow layer of the fault, the weakening effect of the hot water to the fault will be very small, the stress of the fault can continue to accumulate in this area, and the likelihood of strong earthquakes is relatively high. The data in this work show that the circulation depth of the thermal springs in the study area is relatively shallow, so there is still the possibility that moderate or strong earthquakes can occur.

The high geothermal anomaly area is often correlated to mantle material upwelling, which make the crust in an unstable state, and the movement rate varies significantly in such a section, causing the stress to increase and the earthquake to occur. The research results of the velocity structure of the crust and upper mantle in Fujian show that there are obvious east–west and north–south differences in the depth of the Moho discontinuity [59]. From west to east, the thickness of the crust becomes thinner gradually, with a value of 32 km inland and 28 km in coastal areas. The depth of the Moho discontinuity along the coast of Fujian is undulating from south to north, and there are four local uplift areas, namely, the Zhao'an Uplift, Zhangzhou-Xiamen Uplift, Quanzhou Uplift and Fuzhou Uplift. As the Zhangzhou Uplift and Fuzhou Uplift are also two significant geothermal anomalies [60], we deduced that such two areas are also earthquake-prone zones. There are still many discussions on the geothermal source in Fujian. One of these statements is that the magmatic rock heat invaded since the Quaternary may be a heat source for geothermal energy [57], and the high enrichment coefficient of the trace element Mo in the thermal spring we sampled also support this view.

In short, the seismic activity in Fujian is closely related to the distribution of the thermal springs. The distribution density and intensity of the earthquakes increase from west to east and from north to south, which is consistent with the distribution of thermal springs. This consistency is also the result of deep material migration and energy exchange.

A continuous measurement of the main anions and cations were performed in five thermal springs (W03, W04, W12, W23 and W29) every three days since January 2020. The standard deviation was used to characterize the changes in the data, and values exceeding 2σ are regarded as a significant abnormal change. As showed in Figure 7, the curve represents sodium, chlorine, sulfate and TDS for five springs. The ion concentration from the beginning of the observation, although there are fluctuations, basically varied within a small range of the mean value. From the continuous observation data of rainfall (grey histogram), there was little effect on the ion concentration of the thermal springs. The blue bar represents seismic activity within 50 km of each spring. With the exception of the W29 spring, the activity of small earthquakes near the other four springs is relatively dense, but the magnitude of these earthquakes is smaller with the largest one being M_L2.4, and these small seismic activities did not cause a significant change in the ion concentration of the considered springs. In terms of seismic activity within 500 km of the spring point, there were 20 earthquakes of $M \geq 5$ occurring around the Taiwan Strait since January 2020. Of these, there were three $M > 5.5$ earthquakes, namely, the *M*5.8 earthquake in Yilan, Taiwan, on 10 December 2020, and the *M*5.6 and *M*6.1 earthquake in Hualien, Taiwan, on 18 April 2021. The ion concentration of the hot spring did not deviate significantly before almost all the *M*5 earthquakes; however, the TDS of W12 spring increased significantly one month prior to the Yilan *M*5.8 earthquake, and the chloride ion of W03 had a high value close to the abnormal value threshold. There were obviously abnormal changes in the chlorine of four springs, and a high value of abnormal changes in sodium at W12, W23 and W29 springs. Sodium, chlorine, sulfate and TDS at the W29 spring all showed abnormal high-value changes (Table 3). These precursory changes, especially in chlorine concentration, occurred from 85 to 168 days prior to the Hualien *M*6.1 earthquake, which is not accidental in long continuous observations, and are likely to indicate some correlation with seismic activity of *M*6 or above in the Taiwan Strait. The abnormal pre-earthquake changes in the ion concentration of hot springs observed in Fujian are consistent with the findings of some scientists; for example, significant increases in chlorine ions in nearby thermal springs were observed before the 1996 Pyrenees M_L5.2 earthquake [61]. The geochemical anomalies, including changes in the ion concentration of thermal springs before earthquakes, have been summarized, and the possible mechanisms for such changes discussed [62–65].

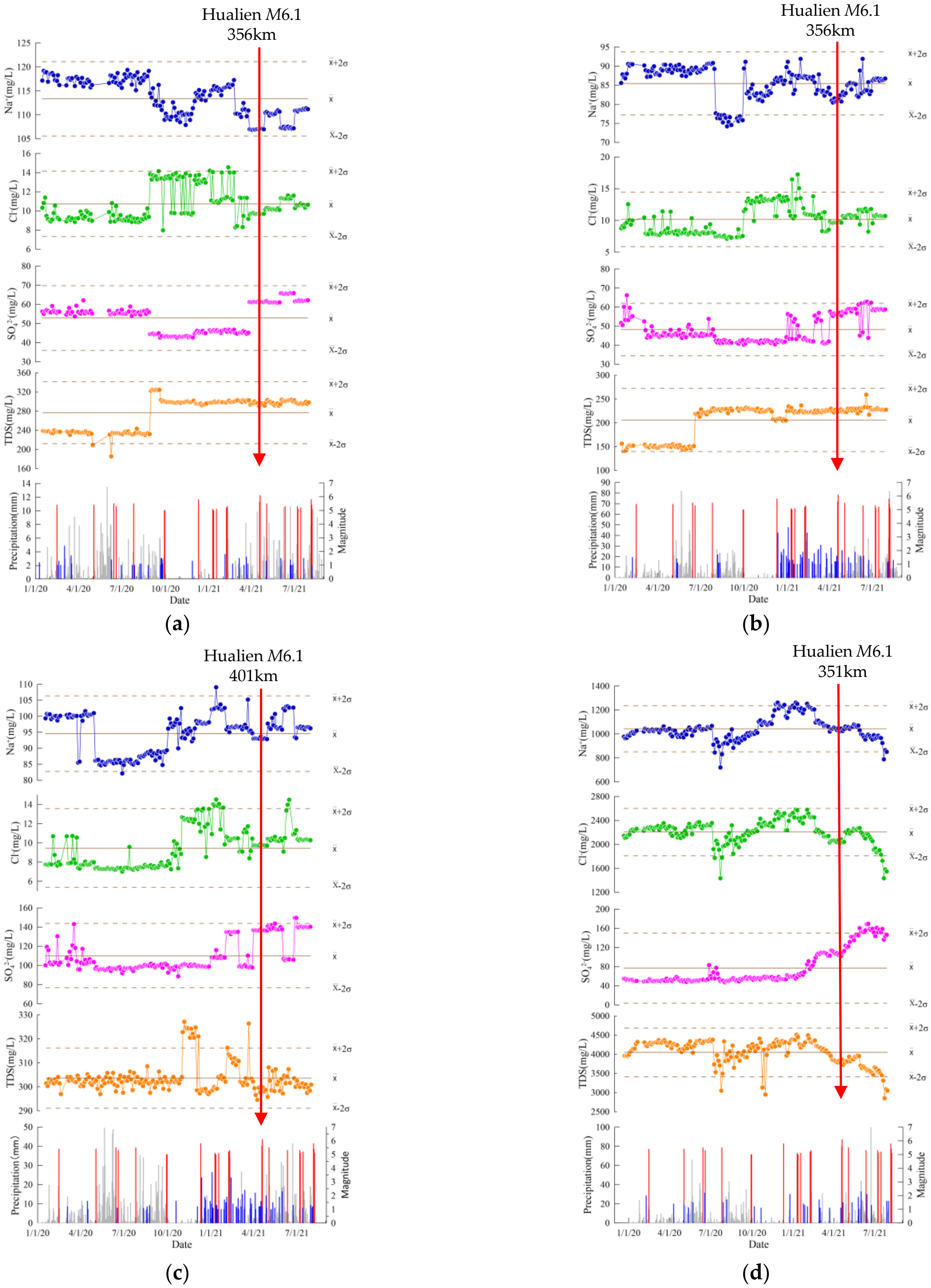

Figure 7. *Cont*.

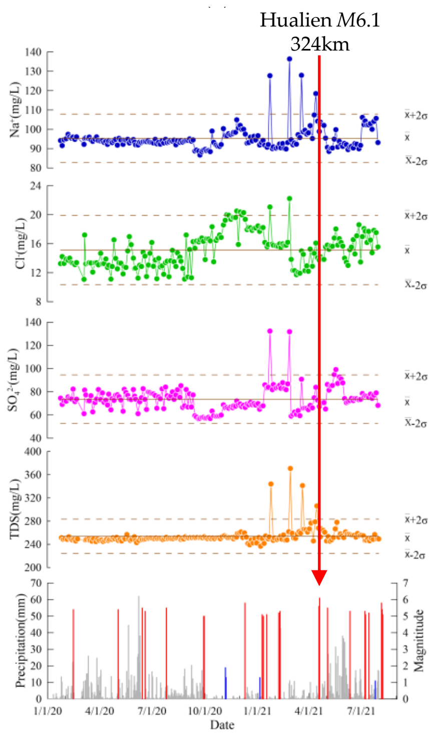

(**e**)

Figure 7. Temporal variations of concentration of Na^{+}, Cl^{-}, SO_4^{2-}, TDS and precipitation: (**a**) the Tadou spring (W03); (**b**) the Longmen spring (W04); (**c**) the Tainei spring (W12); (**d**) the Gangwei spring (W23); (**e**) the Guian spring (W29). Blue bars show the near-field $M_L \geq 1.0$ earthquakes within 50 km and red bars show the far-field $M_S \geq 5.0$ earthquakes with 500 km; gray bars show the daily precipitation.

Table 3. The precursory anomalies of five thermal springs before the Hualien *M*6.1 earthquake on April 18, 2021.

Thermal Spring Code	Precursory Anomalies							
	Na^{+} (mg/L)	Cl^{-} (mg/L)	SO_4^{2-} (mg/L)	TDS (mg/L)	Start Time (YYYY-MM-DD)	Duration (Day)	Variation Range (%)	Epicentral Distance (km)
W03	–	14.20 (10.74)	–	–	2021/1/3	105	32	356
W04	–	16.46 (10.14)	–	–	2021/1/12	96	62	356
W12	109.08 (94.57)		–		2021/1/12	96	15	401
		13.58 (9.46)	–		2020/12/16	123	44	401
			–	322.8 (303.6)	2020/11/1	168	6	401
W23	1248.80 (1043.83)	–	–	–	2020/12/7	132	20	351
W29	127.77 (95.32)		132.39 (73.60)	344.14 (253.72)	2021/1/23	85	34, 80 and 36 respectively	324
		20.00 (15.14)			2020/11/9	160	32	324

The numbers in parentheses represent the average value of the ion concentrations in each thermal spring.

Changes in the regional tectonic stress will alter the circulation system of groundwater, causing fluid mixing or water–rock interaction, leading to abnormal changes in the composition of groundwater. Fault movements and earthquake activity at Fujian and the Taiwan

Strait were controlled by subduction-collision compression of the Pacific plate into the Eurasian plate as well as the Philippine Sea plate to the northwest [66–71], which results in similar dynamics process between Fujian and the Taiwan Strait. So, the circulation system of underground fluids could be affected by the same tectonic stress field at the strong interplate seismic zone in eastern Taiwan, the marginal seismic zone in western Taiwan and the intraplate seismic zone along the southeast coast of Fujian. According to the research results, the strain radius of a *M*6 earthquake can reach 380 km [72], so it could cause fluid mixing, deep fluid upwelling and water–rock reaction intensification when a $M \geq 6$ earthquake within a few hundred kilometers nearby occurs, which would lead to changes in the ion concentration in the thermal springs [73]. This may be one of the reasons why the ion concentration in some thermal springs changed significantly before the Hualien *M*6.1 earthquake. Therefore, continuous hydrochemical monitoring of typical thermal springs in Fujian is of great significance for the short-term and imminent judgment of strong earthquakes in the nearby regions and Taiwan Strait.

5. Conclusions

The distribution of thermal springs and their chemical compositions are affected by the structural characteristics of the fault, the movement rate and the circulation depth of groundwater. The following conclusions were obtained from the analysis of the hydrochemical data in thermal springs of Fujian:

(1) The characteristics of the hydrogen and oxygen isotopes in the thermal springs indicate that precipitation is the main source of recharge for thermal springs in the study area, and the recharge height is 25~1859 m. The geothermal reservoir temperature varies from 90 °C to 226 °C, while the circulation depths of the thermal springs in the study area are relatively shallow, most of which are between 2.9 km and 5.4 km, except for the Xiefang (W10) thermal spring with a circulation depth of 8.4 km.

(2) Na^+ is the main cation while HCO_3^- and SO_4^{2-} are the main anions of the sample springs. The enrichment coefficients of the trace elements Mo and Sr in the thermal springs are greater than 1, and both elements have a typical granite origin. The Sr isotope in thermal springs has obviously different characteristics in the depression belt in southwestern Fujian and the volcanic terrain in eastern Fujian, which indicates the influence of different rock formations on the groundwater cycle process.

(3) Seismic activity is closely correlated to thermal spring distribution in the study area. The density and intensity of earthquakes increase from west to east and from north to south, which is consistent with the distribution of thermal springs. Continuous measurements of the main anions in the five thermal springs showed that the ion concentrations, especially chlorine and sodium, in the thermal springs increased significantly before earthquakes of $M \geq 6$ in the Taiwan Strait and nearby seas. This indicates the possibility of using the ion concentration in thermal spring as a means of earthquake monitoring and prediction.

Supplementary Materials: The following are available online at https://www.mdpi.com/article/10.3390/w13243523/s1, Table S1: Hydrochemistry and stable isotopes in thermal spring samples, Table S2: Trace elements in thermal spring samples.

Author Contributions: Conceptualization, B.W., X.Z. and Y.Z.; methodology, B.W. and X.Z.; software, B.W., J.Z. and F.L.; validation, S.O., Y.Y. and F.L.; formal analysis, B.W. and Y.L.; investigation, S.O., Y.Y. and F.L.; data curation, B.W. and J.Z.; writing—original draft preparation, B.W.; writing—review and editing, B.W., X.Z. and Y.Z.; visualization, B.W. All authors have read and agreed to the published version of the manuscript.

Funding: This research was funded by National Key Research and Development Project (2017YFC1500501-05, 2019YFC1509203) and the National Natural Science Foundation of China (41673106, 42073063, 4193000170) and The Special Fund of the Institute of Earthquake Forecasting, China Earthquake Administration (2020IEF0604, 2020IEF0703, 2021IEF0602, 2021IEF0101, 2021IEF1201) and Spark Program of Earthquake Sciences (XH19055).

Data Availability Statement: The raw data supporting the conclusions of this article will be made available by the authors, without undue reservation.

Acknowledgments: Thanks to Li Liwu and Li Zhongping from the Lanzhou Petroleum Resources Research Center, Institute of Geology and Geophysics, Chinese Academy of Sciences, and Liu Hanbin, Liu Mu, and Liu Xiaotong from the Testing Center of the Nuclear Industry Geology Institute for their help in the elements measurement. The manuscript has benefitted considerably from the appreciated suggestions of two anonymous reviewers.

Conflicts of Interest: The authors declare no conflict of interest.

References

1. Tokunaga, T. Modeling of earthquake-induced hydrological changes and possible permeability enhancement due to the 17 January 1995 Kobe Earthquake, Japan. *J. Hydrol.* **1999**, *223*, 221–229. [CrossRef]
2. Toutain, J.P.; Baubron, J.C. Gas geochemistry and seismotectonics: A review. *Tectonophysics* **1999**, *304*, 1–27. [CrossRef]
3. Tsunogai, U.; Wakita, H. Precursory chemical changes in ground water: Kobe earthquake, Japan. *Science* **1995**, *269*, 61–63. [CrossRef]
4. Kennedy, B.M.; Kharaka, Y.K.; Evans, W.C.; Ellwood, A.; Depaolo, D.J.; Thordsen, J.; Ambats, G.; Mariner, R.H. Mantle Fluids in the San Andreas Fault System, California. *Science* **1997**, *278*, 1278–1281. [CrossRef]
5. Sano, Y.; Takahata, N.; Igarashi, G.; Koizumi, N.; Sturchio, N.C. Helium degassing related to the Kobe earthquake. *Chem. Geol.* **1998**, *150*, 171–179. [CrossRef]
6. Favara, R.; Grassa, F.; Inguaggiato, S.; Valenza, M. Hydrogeochemistry and stable isotopes of thermal springs: Earthquake-related chemical changes along Belice Fault (Western Sicily). *Appl. Geochem.* **2002**, *16*, 1–17. [CrossRef]
7. Hartmann, J. Long-term seismotectonic influence on the hydrochemical composition of a spring located at Koryaksky-Volcano, Kamchatka: Deduced from aggregated earthquake information. *Int. J. Earth Sci.* **2006**, *95*, 649–664. [CrossRef]
8. Du, J.G.; Cheng, W.Z.; Zhang, Y.L.; Jie, C.L.; Guan, Z.J.; Liu, W.L.; Bai, L.P. Helium and carbon isotopic compositions of thermal springs in the earthquake zone of Sichuan, Southwestern China. *J. Asian Earth Sci.* **2006**, *26*, 533–539. [CrossRef]
9. Shi, Z.J.; Shi, Z.M.; Yin, G.; Liang, J.L. Travertine deposits, deep thermal metamorphism and tectonic activity in the Longmenshan tectonic region, southwestern China. *Tectonophysics* **2014**, *633*, 156–163. [CrossRef]
10. Skelton, A.; Andrén, M.; Kristmannsdóttir, H.; Stockmann, G.; Mörth, C.-M.; Sveinbjrnsdóttir, Á.; Jónsson, S.; Sturkell, E.; Gurúnardóttir, H.R.; Hjartarson, H.; et al. Changes in groundwater chemistry before two consecutive earthquakes in Iceland. *Nat. Geosci.* **2014**, *7*, 752–756. [CrossRef]
11. Skelton, A.; Claesson, L.L.; Wästeby, N.; Andrén, M.; Stockmann, G.; Sturkell, E.; Mörth, C.M.; Stefansson, A.; Tollefsen, E.; Siegmund, H.; et al. Hydrochemical changes before and after earthquakes based on long term measurements of multiple parameters at 2 sites in northern Iceland—A review. *J. Geophys. Res. Solid Earth* **2019**, *124*, 2702–2720. [CrossRef]
12. Zhou, X.C.; Wang, W.C.; Chen, Z.; Li, Y.; Liu, L.; Xie, C.; Cui, Y.J.; Du, J.G.; Cheng, J.W.; Yang, L.M. Hot spring Gas Geochemistry in Western Sichuan Province, China After the Wenchuan M_S 8.0 Earthquake. *Terr. Atmos. Ocean. Sci.* **2015**, *26*, 361–373. [CrossRef]
13. Zhou, X.C.; Liu, L.; Chen, Z.; Cui, Y.J.; Du, J.G. Gas geochemistry of the hot spring in the Litang fault zone, Southeast Tibetan Plateau. *Appl. Geochem.* **2017**, *79*, 17–26. [CrossRef]
14. Barberio, M.D.; Barbieri, M.; Billi, A.; Doglioni, C.; Petitta, M. Hydrogeochemical changes before and during the 2016 Amatrice-Norcia seismic sequence (central Italy). *Sci. Rep.* **2017**, *7*, 11735. [CrossRef] [PubMed]
15. Sato, T.; Takahashi, H.A.; Kawabata, K.; Takahashi, M.; Inamura, A.; Handa, H. Changes in the nitrate concentration of spring water after the 2016 Kumamoto earthquake. *J. Hydrol.* **2020**, *580*, 124310. [CrossRef]
16. Nakagawa, K.; Yu, Z.Q.; Berndtsson, R.; Hosono, T. Temporal characteristics of groundwater chemistry affected by the 2016 Kumamoto earthquake using self-organizing maps. *J. Hydrol.* **2020**, *582*, 124519. [CrossRef]
17. Muir-Wood, R.; King, G.C.P. Hydrological signatures associated with earthquake strain. *J. Geophys. Res. Atmos.* **1993**, *98*, 22035–22068. [CrossRef]
18. Wang, C.Y.; Wang, C.H.; Manga, M. Coseismic release of water from mountains: Evidence from the 1999 (Mw 7.5) Chi-Chi earthquake. *Geology* **2004**, *32*, 769–772. [CrossRef]
19. Wang, C.Y.; Manga, M. New streams and springs after the 2014 Mw 6.0 South Napa earthquake. *Nat. Commun.* **2015**, *6*, 7597. [CrossRef] [PubMed]
20. Barbieri, M.; Boschetti, T.; Barberio, M.D.; Billi, A.; Franchini, S.; Iacumin, P.; Selmo, E.; Petitta, M. Tracing deep fluid source contribution to groundwater in an active seismic area (central Italy): A combined geothermometric and isotopic (δ13C) perspective. *J. Hydrol.* **2020**, *582*, 124495. [CrossRef]
21. Tian, J.; Pang, Z.H.; Liao, D.W.; Zhou, X.C. Fluid geochemistry and its implications on the role of deep faults in the genesis of high temperature systems in the eastern edge of the Qinghai Tibet Plateau. *Appl. Geohemistry* **2021**, *131*, 105036. [CrossRef]
22. Shangguan, Z.G. A study on the origin of the fault gas in west Yunnan province. *Earthq. Res. China* **1989**, *5*, 51–56. (In Chinese)
23. Shangguan, Z.G.; Huo, W.G. The δD values of H_2 in the geothermal region of tengchong hot sea and its genesis. *Chin. Sci. Bull.* **2001**, *15*, 1316–1320. (In Chinese)

24. Griffin, S.; Horton, T.W.; Oze, C. Origin of warm springs in Banks Peninsula, New Zealand. *Appl. Geochem.* **2017**, *86*, 1–12. [CrossRef]
25. Wang, F. Zircon U−Pb geochronology, geochemical characteristics and tectonic implications of Caledonian granites from the Xuanhe area, Southwestern Fujian Province. *Geol. China* **2021**, *48*, 207–228. (In Chinese)
26. Zeng, F.; Zhu, J.C.; Zhang, Q.X. Anomaly response of groundwater radon in Fujian province stations to Taiwan strong earthquakes. *Earthquake* **2001**, *21*, 103–106. (In Chinese)
27. Liao, L.X.; Zheng, Y.T.; Yuan, L.W. Analysis on the difference of reflecting characteristics of hydro-radon in Huaan-Tainei well to earthquakes in Fujian and Taiwan region. *Earthquake* **2021**, *30*, 133–139. (In Chinese)
28. Huang, Q.T.; Zheng, S.P. Micro-relief research on active fault in the coast of southeast Fujian and adjacent area. *Prog. Geophys.* **2006**, *21*, 1099–1107. (In Chinese)
29. Chen, Z.; Zhou, X.C.; Du, J.G.; Xie, C.; Liu, L.; Li, Y.; Yi, L.; Liu, H.; Cui, Y.J. Hydrochemical characteristics of thermal spring waters in the Kangding district related to the Lushan M_S7.0 earthquake in Sichuan, China. *Nat. Hazards Earth Syst. Sci. Discuss.* **2015**, *2*, 1149–1156. [CrossRef]
30. Zhang, Y.H.; Zhang, L.S.; Chang, Y.; Fan, Z.W.; Guo, D.F. Determining Trace Elements in Rock Samples Containing Refractory Minerals by Pressurize-microwave Inductively Coupled Plasma Mass Spectrometry. *Uranium Geol.* **2018**, *34*, 105–111. (In Chinese)
31. Liu, H.B.; Jin, G.S.; Li, J.J.; Han, J.; Zhang, J.F.; Zhang, J.; Zhong, F.W.; Guo, D.Q. Determination of stable isotope composition in uranium geological samples. *World Nucl. Geosci.* **2013**, *30*, 174–179. (In Chinese)
32. Tang, S.T.; Wang, X.M.; Cui, J.Y.; Liu, Y.A. Method improvement of selective dissolution of carbonate minerals in whole rock samples and determination of strontium isotopic ratio. *World Nucl. Geosci.* **2015**, *32*, 51–56. (In Chinese)
33. Maloszewski, P.; Zuber, A. Determining the turnover time of groundwater systems with the aid of environmental tracers. 1. models and their applicability. *J. Hydrol.* **1982**, *57*, 207–231. [CrossRef]
34. Han, Z.W.; Tang, C.Y.; Piao, J.Q.; Li, X.; Cao, Y.J.; Matsumaru, T.; Zhang, C.P. Application of chlorofluorocarbons (CFCs) to estimate the groundwater age at a headwater wetland in Ichikawa City, Chiba Prefecture, Japan. *Appl. Water Sci.* **2014**, *4*, 291–302. [CrossRef]
35. Soto-Jiménez, M.F.; Páez-Osuna, F. Distribution and normalization of heavy metal concentrations in mangrove and lagoonal sediments from Mazatlán harbor (SE gulf of California). *Estuar. Coast. Shelf Sci.* **2001**, *53*, 259–274. [CrossRef]
36. Aiuppa, A.; Dongarra, G.; Capasso, G.; Allard, P. Trace elements in the thermal groundwaters of Vulcano island (Sicily). *J. Volcanol. Geotherm. Res.* **2000**, *98*, 189–207. [CrossRef]
37. Richter, F.M.; Rowley, D.B.; DePaolo, D.J. Sr isotope evolution of seawater: The role of tectonics. *Earth Planet. Sci. Lett.* **1992**, *109*, 11–23. [CrossRef]
38. Negrel, P. Water-granite interaction: Clues from strontium, neodymium and rare earth elements in soil and waters. *Appl. Geochem.* **2006**, *21*, 1432–1454. [CrossRef]
39. Wang, Y.S.; Chen, J.S.; Chen, L. Tracing groundwater with strontium isotopic composition in the Hexi corridor basin, northwestern China. *Acta Geol. Sin.* **2007**, *81*, 563–569.
40. Craig, H. Isotopic variations in meteoric waters. *Science* **1961**, *133*, 1702–1703. [CrossRef]
41. Giggenbach, W.F. Isotopic shifts in waters from geothermal and volcanic systems along convergent plate boundaries and their origin. *Earth Planet. Sci. Lett.* **1992**, *113*, 495–510. [CrossRef]
42. Pang, Z.; Kong, Y.; Li, J.; Tian, J. An isotopic geoindicator in the hydrological cycle. *Procedia Earth Planet. Sci.* **2017**, *17*, 534–537. [CrossRef]
43. Yao, X.H.; Cui, P.; Hao, J.M. Use of stable isotope for evaluating washout process in summer at Minnan area. *Environ. Sci.* **1997**, *18*, 13–15. (In Chinese)
44. Cai, M.G.; Huang, Y.P.; Chen, M.; Liu, G.S.; Jin, D.Q.; Zhou, X.H. A study on hydrogen and oxygen isotopes composition of precipitation in Xiamen. *J. Oceanogr. Taiwan Strait* **2000**, *19*, 446–453. (In Chinese)
45. Chen, J.F.; Cao, J.P.; Huang, Y.P. The hydrogen and oxygen isotope composition of precipitation in the Xiamen coastal area. *J. Mar. Sci.* **2020**, *28*, 11–17. (In Chinese)
46. Liu, J.R.; Song, X.F.; Sun, X.M.; Yuan, G.F.; Liu, X.; Wang, S.Q. Isotopic composition of precipitation over Arid Northwestern China and its implications for the water vapor origin. *J. Geogr. Sci.* **2009**, *19*, 164–174. [CrossRef]
47. Giggenbach, W.F. Geothermal solute equilibria: Derivation of Na–K–Ma–Ca geoindicators. *Geochim. Cosmochim. Acta* **1988**, *52*, 2749–2765. [CrossRef]
48. Giggenbach, W.; Sheppard, D.S.; Robinson, B.W.; Stewart, M.K.; Lyon, G.L. Geochemical structure and position of the Waiotapu geothermal field, new zealand. *Geothermics* **1994**, *23*, 599–644. [CrossRef]
49. Fournier, R.O.; Potter, R. Revised and Expanded Silica (Quartz) Geothermometer. *Geotherm. Resour. Counc. Bull.* **1982**, *11*, 10.
50. Fournier, R.O. A revised equation for Na/K geothermometer. *Trans.-Geotherm. Resour. Counc.* **1979**, *3*, 221–224.
51. Fournier, R.O.; Truesdell, A.H. Geochemical indicators of subsurface temperature-Part II, Estimation of temperature and fraction of hot water mixed with cold water. *J. Res. U. S. Geol. Surv.* **1974**, *2*, 263–270.
52. Apollaro, C.; Vespasiano, G.; De Rosa, R.; Marini, L. Use of mean residence time and flowrate of thermal waters to evaluate the volume of reservoir water contributing to the natural discharge and the related geothermal reservoir volume. Application to Northern Thailand hot springs. *Geothermics* **2015**, *58*, 62–74. [CrossRef]

53. Guidi, M.; Marini, L.; Scandiffio, G.; Cioni, R. Chemical geothermometry in hydrothermal aqueous solutions: The influence of ion complexing. *Geothermics* **1990**, *19*, 415–441. [CrossRef]
54. Chiodini, G.; Cioni, R.; Guidi, M.; Marini, L. Chemical geothermometry and geobarometry in hydrothermal aqueous solutions: A theoretical investigation based on a mineral-solution equilibrium model. *Geochim. Cosmochim. Acta* **1991**, *55*, 2709–2727. [CrossRef]
55. Lin, W.J.; Chen, X.Y.; Gan, H.N.; Yue, G.F. Geothermal, geological characteristics and exploration direction of hot dry rocks in the Xiamen ba Zhangzhou basin, southeastern China. *Acta Geol. Sin.* **2002**, *94*, 2066–2077. (In Chinese)
56. Yuan, Y.S.; Ma, Y.S.; Hu, S.B.; Guo, T.L.; Fu, X.Y. Present-day geothermal characteristics in South China. *Chin. J. Geophys.* **2006**, *49*, 1118–1126. (In Chinese) [CrossRef]
57. He, Y.J.; Chen, M.G. Characters and thermal source of thermal springs in Fujian province. *Geol. Fujian* **1999**, *18*, 149–155. (In Chinese)
58. Bear, J. *Dynamics of Fluids in Porous Media*; Elsevier: New York, NY, USA, 1972; 764p.
59. Cai, H.T.; Jin, X.; Wang, S.X.; Li, P.; Chen, W. The crust structure and velocity structure characteristics beneath Ninghua-Datian-Hui'an. *Chin. J. Geophys.* **2016**, *59*, 157–168. (In Chinese)
60. Teng, J.W.; Si, X.; Zhuang, Q.X.; Yan, Y.F.; Zheng, S.G. Fine structure of crust and mantle and potential hot dry rock beneath the Zhangzhou basin. *Chin. J. Geophys.* **2019**, *62*, 1613–1632. (In Chinese)
61. Toutain, J.P.; Munoz, M.; Poitrasson, F.; Lienard, A.C. Springwater chloride ion anomaly prior to a M_L = 5.2 Pyrenean earthquake. *Earth Planet. Sci. Lett.* **1997**, *149*, 113–119. [CrossRef]
62. Thomas, D. Geochemical precursors to seismic activity. *Pure Appl. Geophys.* **1988**, *126*, 241–266. [CrossRef]
63. Martinelli, G.; Tamburello, G. Geological and Geophysical Factors Constraining the Occurrence of Earthquake Precursors in Geofluids: A Review and Reinterpretation. *Front. Earth Sci.* **2020**, *8*, 596050. [CrossRef]
64. Quattrocchi, F.; Pik, R.; Pizzino, L.; Guerra, M.; Lombardi, S. Geochemical changes at the Bagni di Triponzo thermal spring during the Umbria-Marche 1997-1998 seismic sequence. *J. Seismol.* **2000**, *4*, 567–587. [CrossRef]
65. Wang, C.; Manga, M. *Water and Earthquakes*; Springer: Berlin/Heidelberg, Germany, 2001. [CrossRef]
66. Angelier, J.; Bergerat, F.; Chu HT, L.; Lee, T.Q. Tectonic analysis and the evolution of a curved collision belt: The Hsuehshan range, northern Taiwan. *Tectonophysics* **1990**, *183*, 77–96. [CrossRef]
67. Liu, C.C.; Yu, S.B. Vertical crustal movements in eastern Taiwan and their tectonic implications. *Tectonophysics* **1990**, *183*, 111–119.
68. Yu, S.B.; Chen, H.Y.; Kuo, L.C. Velocity field of GPS stations in the Taiwan area. *Tectonophysics* **1997**, *274*, 41–59. [CrossRef]
69. Ching, K.E.; Rau, R.J.; Lee, J.C.; Hu, J.C. Contemporary deformation of tectonic escape in SW Taiwan from GPS observations 1995–2005. *Earth Planet. Sci. Lett.* **2007**, *262*, 601–609. [CrossRef]
70. Zhou, S.Y.; Wu, Y.; Qin, X.J.; Shuai, P.; Shi, S.Y.; Deng, G.J.; Zhou, X. Study on the crustal horizontal movement in Fujian and its neighbouring sea region in 1994 to 1997 based on several kinds of GPS surveying data. *Chin. J. Geophysics* **2000**, *43*, 471–479. (In Chinese) [CrossRef]
71. Yang, X.Q.; Shi, X.B.; Xu, H.H. Numerical modeling of the current tectonic stress field in Taiwan strait and its adjacent regions. *Chin. J. Geophys.* **2012**, *55*, 2307–2318. (In Chinese) [CrossRef]
72. Dobrovolsky, I.P.; Zubkov, S.I.; Miachkin, V.I. Estimation of the size of earthquake preparation zones. *Pure Appl. Geophys.* **1979**, *117*, 1025–1044. [CrossRef]
73. Martinelli, G. Previous, current, and future trends in research into earthquake precursors in geofluids. *Geosciences* **2020**, *10*, 189. [CrossRef]